Anisotropy Analysis in Shale Using Advanced Sonic Data - Bakken Case Study*

Mehdi Ostadhassan[1], Zhengwen Zeng[1], and Hadi Jabbari[1]

[1]University of North Dakota, Grand Forks, ND (mehdi.ostadhassan@my.und.edu)

Abstract

Incorporating anisotropy in seismic data processing will improve accuracy in prestack depth migration, amplitude variation with offset (AVO) and hydraulic fracture monitoring, among which hydraulic fracing plays a critical role in production enhancement of tight reservoirs such as Bakken Formation. Considering shales as being vertically transverse isotropic (VTI), three Thomsen anisotropy parameters with five independent stiffness coefficients could be used to fully characterize them. So far, different methods are applied to measure these parameters directly such as walkaway vertical seismic profiling (VSP), multi-offset and multi-azimuthal VSP. Although these surveys can provide us reliable anisotropic models, various constraints including the cost could limit recording the VSPs. Recent innovations in the acquisition of broadband sonic waveforms and dispersion analysis have changed the industry's perspective on cost of anisotropy analysis.

In this paper, advanced sonic data in two producing wells in the Bakken Formation, each drilled through different geologic features has been acquired and analyzed. One is located on the crest of Nesson anticline, the major geologic structure in the area. The other is away from the anticline and none of the Nesson geologic feature is visible. First, five stiffness moduli were estimated from the Stoneley, two flexural waves and formation density. Second, the Thomsen parameters in three members (upper, middle and lower) of Bakken were calculated and compared one another. It has been found that the Upper and Lower Bakken are highly VTI because of the clay platy particles, while the middle member is isotropic or slightly anisotropic. The well on the top of the anticline shows a higher degree of anisotropy in the middle member; and we interpreted this as the presence of fractures due to the folding. Finally, data inversion of Stoneley and two flexural waves was performed to create slowness radial profile around the borehole and in the far field

to elaborate the idea of existence of intrinsic fractures and to discriminate them from the drilling induced ones. The well on the crest of the anticline shows higher amount of variations in the Stoneley wave slowness. Stoneley wave is proved to be sensitive to the mobility and could be an indicator of higher permeability.

Introduction

Velocity anisotropy is a key parameter for seismic data processing and interpretation. Most of the rock constituents of the earth's crust exhibit some degree of anisotropy. Anisotropy is defined as the variation of a physical property with respect to the direction of measurement; either the direction of propagation or polarization of waves (Tatham and McCormack, 1991). Anisotropy of sedimentary sequences originates from different factors, such as the preferred orientation of minerals or grain particles, which is known as intrinsic anisotropy, a sequence of thin isotropic layers, and finally stress-induced anisotropy which initiates from fracture alignment (Thomsen 1986). Generally speaking, anisotropy in rocks can be characterized either as intrinsic or stress induced (Jaeger and Cook, 1977).

Shales are major component of sedimentary basins (Hornby, 1994) and exhibit a high degree of intrinsic anisotropy due to their microstructures and platy shape clay minerals (Sayers, 2005). In fact, shales could be described by making some assumptions that lead to a specific type of isotropic medium known as Vertically Transverse Isotropy (VTI) (Sayers, 1994; Vernik and Liu, 1997). This has made transverse isotropy the most common anisotropy model in exploration seismology. Neglecting anisotropy in shales may lead to crucial errors in normal move-out (NMO) corrections; dip move-out (DMO) corrections, migration, and amplitude variation with offset (AVO) analysis.

Theory

Vertical transverse isotropy, also known as polar anisotropy (Walsh et al., 2006), can be quantified in the manner of including transverse isotropic planes with vertical axis of rotational symmetry. A VTI medium can be well characterized by having five independent elastic stiffness coefficients. In addition, a VTI medium could also be quantified with the estimation of three dimensionless anisotropy parameters, epsilon (ε), gamma (γ) and delta (δ) (Thomsen, 1986). In this regard, considering x_3 as the axis of rotational symmetry in the conventional two index notation (Nye, 1985, Higgins et al., 2008) and applying general Hook's law (eq. 1), the non-vanishing elastic stiffness coefficients (eq. 3) of the elasticity matrix (eq. 2) reads as follows:

$$\sigma_{ij} = C_{ijkl}\varepsilon_{kl} - \alpha P_p \dots\dots\dots\dots\dots\dots\dots\dots\dots\dots\dots\dots\dots\dots\dots\dots\dots\dots\dots\dots\dots(1)$$

Where σ_{ij}: Stress tensor, C_{ijkl}: Fourth rank stiffness tensor, ε_{kl}: Strain tensor, α: Biot's constant and P_p: Pore pressure, and the conventional two index notation (Nye, 1985) of the stiffness tensor will be:

$$C_{ij} = \begin{pmatrix} C_{11} & C_{12} & C_{13} & 0 & 0 & 0 \\ C_{21} & C_{22} & C_{23} & 0 & 0 & 0 \\ C_{31} & C_{32} & C_{33} & 0 & 0 & 0 \\ 0 & 0 & 0 & C_{44} & 0 & 0 \\ 0 & 0 & 0 & 0 & C_{55} & 0 \\ 0 & 0 & 0 & 0 & 0 & C_{66} \end{pmatrix} \dots\dots\dots\dots\dots\dots\dots\dots\dots\dots\dots\dots\dots\dots\dots\dots\dots(2)$$

and for a VTI medium, the five non-vanishing elastic stiffness coefficients along with C_{66} are as follows:

$$C_{11} = C_{22} , C_{33}, C_{12} = C_{21}, C_{13} = C_{23} = C_{32} = C_{31}, C_{44} = C_{55}, C_{66} = \frac{C_{11} - C_{12}}{2}\dots\dots\dots\dots\dots\dots\dots(3)$$

Thomsen (1986) developed the idea of parameterization of the elastic properties of a TI medium in order to elaborate on diagnostic principles leading to a better understanding of anisotropy from isotropy. Thomsen anisotropy parameters for a TI medium can exactly be illustrated through the vertical propagating compressional and shear wave velocities along the axis of rotational symmetry (x_3) and three dimensionless anisotropic parameters (eq. 4) defined as follows:

$$\epsilon = \frac{C_{11} - C_{33}}{2C_{33}}, \gamma = \frac{C_{66} - C_{55}}{2C_{55}}, \delta = \frac{(C_{13} + C_{55})^2 - (C_{33} - C_{55})^2}{2C_{33}(C_{33} - C_{55})}\dots\dots\dots\dots\dots\dots\dots\dots\dots\dots\dots\dots(4)$$

Epsilon (ϵ) stands for the fractional difference between horizontal (C_{11}) and vertical (C_{33}) P-wave velocities showing P-wave anisotropy. Similarly, gamma (γ) measures the same characteristic for S-wave, which is the difference between the horizontally polarized (C_{66}) and vertically polarized (C_{44}, C_{55}) shear wave. In contrast to the simple definition of ϵ and γ, δ is a more complicated combination of elastic stiffness coefficients. As Thomsen (1986) described, δ is the difference between the smallest offset NMO velocity and vertical velocity to interpret the small AVO response (Tsvankin, 1997). Based on the fact that in an isotropic medium the density is uniform throughout the material and the waves velocity does not change with respect to the direction of propagation,

considering the combination of (eq. 4) and (eq. 5), epsilon (ε), gamma (γ) and delta (δ) will approach zero for an isotropic medium, otherwise their value could represent as the strength of anisotropy (Tsvankin, 2005).

Considering the velocity v_{ij} of an elastic wave traveling along the X_i axis and polarizing along the X_j, the relationship between v_{ij} and C_{ij} for a TI medium will become:

$$v_{11} = v_{22} = \sqrt{\frac{C_{11}}{\rho}}, \ v_{33} = \sqrt{\frac{C_{33}}{\rho}}, v_{12} = v_{21} = \sqrt{\frac{C_{66}}{\rho}}, v_{13} = v_{31} = v_{23} = v_{32} = \sqrt{\frac{C_{55}}{\rho}} \dots\dots\dots\dots\dots\dots\dots\dots\dots\dots\dots (5)$$

where ρ is the bulk density, v_{12} is the velocity of a shear wave propagating along the axis (x_1) and polarized along the axis (x_2), v_{33} is the velocity of a compressional wave traveling along the axis of symmetry (x_3) and polarized along the same axis.

Similar research shows that VSP data, such as walkaway, multi-offset, and multi-azimuth recordings are the most suitable set of data which precisely measures the anisotropy of a formation (Miller and Spencer, 1994; Leany et al., 1999). However, due to various constraints these set of data may not be available. Over the past few years new developments in the field of sonic logging have made the evaluation of shale anisotropy more accurate (Pistre et al., 2005; Walsh et al., 2006). Cross-dipole sonic logging is a powerful instrumentation to detect shear wave velocity anisotropy in a formation (Plona et al., 2000). Furthermore, advanced frequency domain processing of cross-dipole data (slowness frequency analysis or dispersion analysis) had enabled us to identify the formation anisotropy - either intrinsic or stress induced anisotropy (Plona et al., 2002).

Cross-dipole sonic logging along with dispersion curve fitting can measure the fast and slow shear wave velocities caused as a result of shear splitting and radial variation of shear speed into the formation (Esmersoy et al., 1994; Esmersoy et al., 1995; Burridge and Sinha, 1996). If cross-dipole and Stoneley wave measurements are available, an accurate evaluation of transverse isotropic medium can be accomplished (Pistre, 2005). For vertical wells with flat bedding planes, C_{33} represents the vertically propagating P-wave, while C_{44} and C_{55} are the two formation shear moduli of a TI medium, which can be measured by flexural probes. C_{44} and C_{55} are measured in two straight perpendicular planes along the borehole axis. Ultimately, C_{66} is recordable in the plane perpendicular to the borehole axis from the Stoneley tube wave velocity (Norris and Sinha, 1993; Walsh et al., 2007).

For a vertical well as shown in Figure 1, X_3, the axis of symmetry is assumed to be along the borehole axis. This assumption is made when the well is vertical going perpendicular through 0° dipping formation layers, whereas for dipping layers the assumptions will differ. Thus, the formation is azimuthally isotropic in the X1–X2, plane. As shown in Figure 1, C_{44} and C_{55} are the two moduli

corresponding to the fast and slow shear waves, obtained from the dipole flexural modes. Consequently, for a VTI medium we expect $C_{44} = C_{55}$ and C_{66} will be horizontally polarized shear wave from the low frequency asymptote dispersion (Pistre et al., 2005; Walsh et al., 2006), with some corrections (Sinha et al., 2005).

As shown in (eq. 1- 3), in order to entirely characterize VTI medium, five independent elastic moduli are needed; As previously noted, in the vertical wells perpendicular to the bedding plane, only three of these five moduli (C_{33}, C_{44}, and C_{66}) could be measured by advanced sonic logging. Therefore, ANNIE model, a simple assumption has been proposed (Shoenberg et. al., 1996) to estimate the two remaining elastic parameters C_{11} and C_{13}. This is derived as a result of seismic observations that NMO velocity compared to vertical velocities are small, thus Thomsen δ can be set to zero (eq. 6).

$$C_{13} + 2C_{44} - C_{33} = 0, \quad \dots\dots\dots\dots\dots\dots\dots\dots\dots\dots\dots\dots\dots\dots\dots\dots\dots\dots\dots\dots\dots\dots\dots\dots\dots\dots\dots\dots\dots\dots\dots(6)$$

Note that C_{44} and C_{55} can be replaced by one another for a VTI medium in (eq. 6). The second assumption is that for many types of shale $C_{13} = C_{12}$ resulting in (eq. 7):

$$C_{13} = C_{12} = C_{11} - 2C_{66}, \quad C_{66} - C_{44} = \frac{C_{11} - C_{33}}{2} \quad \dots\dots\dots\dots\dots\dots\dots\dots\dots\dots\dots\dots\dots\dots\dots\dots\dots\dots\dots\dots\dots\dots\dots\dots\dots(7)$$

This allows us to express (eq. 8):

$$(C_{11}, C_{13}) = f(C_{33}, C_{44} \ \& \ C_{66}) \quad \dots\dots\dots\dots\dots\dots\dots\dots\dots\dots\dots\dots\dots\dots\dots\dots\dots\dots\dots\dots\dots\dots\dots\dots\dots\dots\dots(8)$$

Geological Setting

Williston Basin, which covers North Dakota, parts of Montana, South Dakota in USA, Manitoba and Saskatchewan in Canada, is considered as an intracratonic basin. The deepest part of the basin in North Dakota, which is 16,099 ft., reaches the age of Cambrian to Tertiary (Pitmen et al, 2001). Regarding stratigraphy of the sediments, various sedimentary facies such as carbonates, clastics and evaporates are recognizable in sets of transgressions and regressions.

Bakken Formation, the rock unit under study, estimated to be late Devonian to early Mississippian, is a shaly formation overlying the Devonian Three Forks Formation, and underlies the Mississippian Lodgepole Formation. The Bakken Formation is well distinguished

with three major members known as Upper Bakken (UB), Lower Bakken (LB) and Middle Bakken (MB) that are well identified from the sharp gamma ray responses. Organic rich marine shales are the major constituent of LB and UB, whereas MB is a mixture of clastic and carbonates. The maximum thickness of the Bakken Formation in North Dakota is reported to be as high as 160 ft (LeFever, 2008).

The Nesson anticline as the main structural geologic feature in North Dakota portion of Williston Basin, trending north-south, is located where MB comes to its maximum thickness. Likewise, the depocenter of the basin in North Dakota exists on the eastern side of the Nesson anticline (LeFever, 2008). Regarding the petroleum potential and petroleum system, Upper and Lower Bakken are both acting as the source and seal for the middle member; therefore, we can say the generated and expelled hydrocarbons have migrated to the middle member (Price and LeFever, 1994). Middle Bakken as the producing section of the formation varies in lithology, changing from calcareous siltstone to dolomite and limestone (Pitman et al., 2001; LeFever, 2008).

Methodology

Figure 2 depicts the location of the two vertical wells from which the sonic data were taken. A powerful tool called the sonic scanner facilitated the sonic logging in such open hole wells when they are filled with fluid (Pistre et al., 2005). As seen in Figure 2, Well A is on top of the Nesson anticline while well B is far away where no geological evidence of the Nesson anticline exists. The depths under study for Well A and B are 10,294 ft to 10,430 ft and 9,715 ft to 9,812 ft, respectively.

Compressional, shear, Stoneley and flexural wave slowness were obtained at different depths of investigation in the formation through short and long spacing sets of sources and receivers. Monopole source can generate non-dispersive P-waves, dispersive S-waves and low frequency slightly dispersive Stoneley waves. Dipole transmitters generate a chirp with a frequency sweep or flexural modes (Arroyo et al., 2006). These waves' slowness measurements resulted in different values in three separate planes, two along the borehole axis and one orthogonal to the wellbore. In addition, dispersion data (slowness vs. frequency) was derived for each set of wave modes for further anisotropy type analysis. Finally, the inversion of slowness data was performed for radial profiling (Sinha et al., 2006) for fluid flow analysis.

Advanced data processing using Best-Delta-Time module of Geoframe (Mark of Schlumberger) software was carried out as the following (Halderson et al., 2006; Arroyo et al., 2006):

- 4-component Alford rotation of fast and slow S-wave for shear anisotropy analysis (Alford, 1986).

- Dispersion curve analysis in order to identify type of anisotropy, either intrinsic or stress induced.
- 3D anisotropy processing of flexural waves to calculate C_{44} and C_{55} in vertical plane from the shear data along the borehole axis, C_{66} from Stoneley wave in horizontal plane, perpendicular to the borehole axis, and C_{33} from compressional data (Figure 1).
- Dipole radial profiling for near wellbore and far offset formation evaluation.

Using eq. 5, the average value of the stiffness coefficients, plus the epsilon and gamma anisotropy parameters for Well A, in the three different members of Bakken Formation (UB, MB and LB) were calculated (Table 1). C_{33}, C_{44}, C_{55} and C_{66} were obtained from the direct measuring of the compressional, shear flexural and Stoneley wave's velocities within the formation along with the formation density. C_{44} and C_{55} are elastic stiffness moduli in vertical planes parallel and perpendicular to the fast shear azimuth. C_{11} is calculated through ANNIE model assumptions using (eq. 6- 8), utilizing C_{44} and C_{55}. The next step is to derive epsilon and gamma using (eq. 4), the two dimensionless anisotropy parameters. In order to derive epsilon and gamma, C_{44} and C_{55} were used interchangeably.

Discussion

From Table 1, it is seen that $C_{44} \neq C_{55} \neq C_{66}$ introducing another type of anisotropic behavior also known as orthorhombic isotropy. In other words, $C_{44} < C_{55}$ for the whole Bakken, this is evidence that dipole shear slowness in two orthogonal sagittal planes along the borehole axis is different. This difference is possibly caused by vertically aligned fractures from stress differences in the cross sectional plane perpendicular to the borehole axis causing shear splitting. C_{55} represents the fast shear azimuth, which is assumed to be in the direction of maximum horizontal stress; and C_{44} in the perpendicular plane representing slow shear wave direction and the direction of minimum horizontal stress crossing the borehole.

The average difference between C_{44} and C_{55} for the middle member is somehow greater than the same difference values for upper and lower members (Table 1). This can be an indication of more open fractures in the middle member than that in the lower and upper members. In addition, the main reason that $C_{44} \neq C_{55}$ in UB and LB - which are playing the role of source rock for Bakken petroleum system - is that they contain high amounts of Total Organic Carbon (TOC), other than the occurrence of the fractures.

Table 2 presents the average anisotropy parameters of the three Bakken members in Well A by definition, epsilon and gamma are interpreted as the fractional difference of vertical and horizontal traveling, compressional and shear waves (Tsvankin, 2005). From Table 2 the following are deduced:

- Positive values of epsilon and gamma are seen for both UB and LB standing for the shale anisotropy. This anisotropy is a combination of shale microlayering and high concentrations of TOC.
- Negative values of epsilon and gamma for MB strongly denote a permeable formation (Pistre, 2005; Walsh et al., 2006).This originates from the presence of horizontal fluid filled fractures acting as barriers to the vertical traveling wave. Although these values are small (Table 2), neglecting them will lead to consider Mb as an isotropic medium (Fang, 2010), thus missing the permeable pay zone.

Dispersion Plot and Radial Slowness Variation Profiling (RSVP)

In order to determine the type of anisotropy, dispersion analysis seems inevitable (Plona et al, 2002; Arroyo et al., 2006). Dispersion plots are graphical representations of frequency versus slowness for the different wave types. In such graphs, slowness in high frequency represents near wellbore, while far field slowness is related to the low frequency region. Dispersion plot enables us to determine whether the formation is isotropic or anisotropic, homogeneous or inhomogeneous. In this regard, four different cases can be created as follows:

1. Homogeneous-isotropic: No shear splitting happens; two recorded flexural wave dispersion curves match each other and overlie the modeled curves.
2. Inhomogeneous-isotropic: both fast and slow flexural modes match each other but shows different slowness with modeled curves at high frequency (near wellbore).
3. Homogeneous-anisotropic: in such condition for intrinsic anisotropy, for instance, shales and microlayering in a VTI medium with borehole axis along the axis of symmetry, flexural modes match each other, but do not overlie the modeled curves. They merge to the true slowness at zero frequency (Arroyo et al., 2006).
4. Inhomogeneous-anisotropic: the two flexural dispersion curves cross each other as a result of stress induced anisotropy.

Radial slowness variation profiles (RSVP) (Sinha et al., 2006 and 2007) are beneficial for formation characterization. Compressional, shear, and Stoneley wave slowness variations in a deep penetration into the formation provide valuable information of true formation properties. Compressional slowness radial variation is obtained from the difference in P-wave slowness detected from far and near offset monopole transmitters (Arroyo et al., 2006). Dipole slowness radial profile (DRP), (red and blue curves in Figure 3b, Figure 4b, Figure 5b, Figure 6b, Figure 7b and Figure 8b) are constructed from the inversion of the difference between measured and modeled slowness at large selection of frequency interval (Sinha et al., 2005, and 2006). Stoneley shear radial profiling (SRP), (green dashed line in Figure 3b, Figure 4b, Figure 5b, Figure 6b, Figure 7b and Figure 8b) is the outcome of the inversion of the differences between

the measured and Stoneley dispersion responses of a reference homogeneous-isotropic formation (Sinha et al., 2006). SRP analysis is a powerful technique that delivers direct continuous information of formation mobility (Brie et al., 1998).

Dispersion and RSVP plots are related to three different depths of the Bakken Formation each of which represents a member of the formation in Well A (Figure 3, Figure 4 and Figure 5). Figure 3a displays the dispersion plot at depth 10,304 ft., which corresponds to UB in Well A that the fast and slow shear flexural modes overlie on each other but do not match the modeled curves. This validates the assumption that the Bakken Formation is more likely to be homogeneous and vertically transverse isotropic. This anisotropy originates from the platy shape clay particles as the major constituent minerals of the shaly UB. As earlier mentioned, shales are known as the best candidates for transverse isotropy. However, our observations shown in Table 1 imply that $C_{44} \neq C_{55}$, thereby not quite matching the results concluded from dispersion plots, in contradiction to our assumption that UB is a VTI medium. Considering UB being VTI concluded from interpreting the dispersion plots. Reconsidering the low frequency region of dispersion plot in Figure 3a, some degree of separation on each of both modeled curves and flexural modes can be observed. Since the difference between C_{44} and C_{55} in Table 1 is not significant, we may yet consider the UB as VTI and not orthorhombic isotropy; similarly LB demonstrates the same behavior as well (Table 1 and Figure 5a). It should also be noted that the values shown in Table 1 are the averages of elastic moduli, and do not represent the exact value for the corresponding depths in Figure 3a, Figure 4a and Figure 5a.

Alternatively, the dispersion plot of middle member (Figure 4a), exhibit a perfect match between the flexural modes and the modeled curves, indicating homogeneous isotropic medium. Considering the RSVP plot in Figure 4b, the mismatch of Stoneley slowness with the overlying flexural modes (slower Stoneley compared to faster shear dipoles) confirms the idea of a quiet permeable Middle Bakken. This confirms the negative outcome of epsilon and gamma in Table 2 for Well A through the MB section. Figure 3b and Figure 5b, show the RSVPs for UB and LB. As was expected, Stoneley slowness was found to be less than the shear dipole slowness, confirming $C_{66} > (C_{44})$ and (C_{55}), and making UB and LB being a VTI material. Additionally, it can be observed in the same figures that the fast and slow shear slowness curves do not match completely, which resulted in $C_{44} \neq C_{55}$.

The same analysis was performed for the advanced sonic data acquired in Well B for the Bakken Formation. The four shear moduli (C_{33}, C_{44}, C_{55} and C_{66}) were directly measured and through ANNIE model assumptions, C_{11} was calculated from (eq.7, 8). The results are summarized in Table 3. Thomsen anisotropy parameters, epsilon and gamma, are derived from the measured and calculated stiffness coefficients and are shown in Table 4. Dispersion and RSVP plots through the previously mentioned data processing workflow (Halderson et al, 2006, Arroyo et al., 2006 and Sinha et al, 2006) are generated and developed. Figure 6, Figure 7 and Figure 8 are the graphical presentation of such plots for Upper, Middle and Lower Bakken in Well B, respectively.

From the average value of stiffness moduli for the three members of Bakken summarized in Table 3, we can see that the measured C_{44} and C_{55}, corresponding to the shear stiffness coefficients in two perpendicular sagittal planes, are close to each other for the whole section. This mathematically results in equality for C11 derived by ANNIE model from either C_{44} or C_{55}. $C_{44} = C_{55}$ illustrates that the dipole shear slowness is behaving isotropic. In comparison to C_{44} or C_{55}, the greater C_{66} in UB and LB indicates transverse isotropy with vertical axis of symmetry parallel to the borehole axis. $C_{44} = C_{55} < C_{66}$ is the verification of no shear splitting, no vertical fracture existence and no fluid mobility (Walsh et al., 2006; Sinha et al., 2006). Fluid mobility in a horizontal plane will lower the C_{66} comparing to C_{44} and C_{55}. For the middle member, $C_{44} = C_{55} = C_{66}$ matches the isotropic characteristics of this interval. Isotropic behavior of MB is confirmed by Table 4, where epsilon and gamma computed from either of C_{44} or C_{55} are negligible and very close to zero. It is worth mentioning that, UB and LB showing strong anisotropy with P-wave anisotropy close to 30% for UB and 26% for LB calculated from (eq. 4). In addition S-wave anisotropy computed being 46% and 40% for UB and LB respectively, (eq. 4).

Comparing the epsilon and gamma estimated from Well A and Well B, and considering the concept of Thomsen parameters, it is concluded that the greater magnitude of those parameters in Well B than those of Well A, may be caused by the pure VTI effect of shales in Bakken Formation in the corresponding well. This could be interpreted that no vertical fractures exist in Well B. In Well A, the presence of vertical fractures resulted in smaller fractional differences of horizontally and vertically propagating P and S waves. The other strong evidence proving the presence of vertical fractures in Well A, specifically in middle member is that epsilon and gamma are negative compared to $\varepsilon = \gamma = 0$ in Well B. The same conclusion could be made when comparing the stiffness moduli from Table 1 and Table 3. The MB in Well A, showing $(C_{44} \neq C_{55}) < C_{66}$ originated from fluid mobility and vertical fractures, whereas MB in Well B is isotropic $(C_{44} = C_{55} = C_{66})$.

Figure 6 and Figure 8 show the dispersion and RSVP plots at depths 9,720 ft and 9,808 ft in Well B. They represent perfect VTI caused by clay minerals in shale in UB and LB. In Figure 6 and Figure 8, flexural modes overlie on each other and do not match the modeled curves in dispersion plots. On the RSVP plots, flexural modes slowness does not separate and are slower than the Stoneley waves. Dispersion and RSVP plots of MB shown in Figure 7 have the responses of an isotropic medium.

Summary

1. Nesson anticline as the major geologic feature in the North Dakota part of Williston Basin has caused vertical fractures in the Bakken Formation. Higher mobility and slight orthorhombic isotropy in the Bakken Formation are the results of Nesson folding. These latest properties are well studied from borehole advanced sonic log data in the region.

2. Advanced sonic logging measurement is a powerful method for elastic stiffness characterization, and anisotropy type analysis. Study of independent shear moduli along with Thomsen anisotropy parameters - evaluated in two vertical wells in North Dakota - infers that the influence of structural geology on shear anisotropy is significant.
3. In Well A, the relationships $(C_{44} \neq C_{55}) > C_{66}$ and $(\varepsilon \neq \gamma < 0)$ resulted from anisotropy analysis - signify the presence of fractures along the Nesson anticline within the middle Bakken member. It can also be inferred that the slight orthorhombic isotropy in LB and UB confirms the fracture extension into these members which yields $(C_{44} \neq C_{55}) < C_{66}$.
4. Applying dispersion plot analysis and radial slowness variation profiling to the cross-dipole sonic data taken from two Bakken wells, fluid mobility and shear anisotropy in a tight reservoir, such as the Bakken formation were successfully characterized.

Acknowledgements

References

Alford, R., 1986, Shear data in the presence of azimuthal anisotropy: Dilley, Texas: 56th SEG annual meeting, Houston, Texas, 2-6 November 1986, expanded abstracts, 4 p.

Arroyo, F., J. Marcedo Ortiz, G. De, L. Renlie, and S. Williams, 2006, Sonic investigations in and around the borehole: Oilfield Review, v. 18, p. 14-33.

Brie, A., D. Johnson, and F. Pampuri, 1998, Quantitative formation permeability evaluation from Stoneley waves: SPE Annual Technical Conference and Exhibition (ATCE), New Orleans, Louisiana, 27-30 September 1998, SPE49131, p. 389-400. doi:10.2118/49131-MS.

Burridge, R., and B. Sinha, 1996, Inversion for formation shear modulus and radial depth of investigation using borehole flexural waves: SEG Annual Technical Conference and Exhibition (ATCE), 66th annual meeting, Denver, Colorado, 10-15 November 1996, expanded abstract, 4 p.

Esmersoy, C., A. Boyd, M. Kane, and S. Denoo, 1995, Fracture and stress evaluation using dipole shear anisotropy logs: SPWLA 36th annual logging symposium.

Esmersoy, C., K. Koster, M. Williams, A. Boyd, and M. Kane, 1994, Dipole shear anisotropy logging: SEG 64th annual meeting, 23-28 October 1994, expanded abstract, 4 p.

Higgins, S., S. Goodwin, Q. Donald, A. Donald, T. Bratton, and G. Tracy, 2008, Anisotropic stress models improve completion design in the Baxter shale: SPE Annual Technical Conference and Exhibition, 21-24 September 2008, Denver, Colorado, SPE 115736-MS, 10 p. doi:10.2118/115736-MS.

Halderson, J., D. Johnson, T. Plona, B. Sinha, H. Valero, and K. Winkler, 2006, Borehole acoustic waves: Oilfield review, v. 18/1, p. 34-43.

Hornby, B.E., 1994, The elastic properties of shales: PhD thesis, University of Cambridge, Cambridge, Massachusetts, 201 p.

Jaeger, J.C., and N.W.G. Cook, 1979, Fundamentals of rock mechanics, 3rd edition: Chapman & Hall, New York, 593 p.

Leany, W.S., C.M. Sayers, and D.E. Miller, 1999, Analysis of multi-azimuthal VSP for anisotropy and AVO: Geophysics, v. 64, p. 1172-1180.

LeFever, J., 2008, Isopach of the Bakken Formation: North Dakota Geological Survey, geologic investigations 59, Bakken Formation map series, scale 1:1000000.

Miller, D.E., and C. Spencer, 1994, An exact inversion for anisotropic moduli from phase slowness data: Journal of Geophysical Research, v. 99, p. 21651-21657.

Norris, A., and B. Sinha, 1993, Weak elastic anisotropy and the tube wave: Geophysics, v. 58, p. 1091-1098.

Nye, J.F., 1985, Physical properties of crystals: their representation by tensors and matrices: Oxford University Press, Clarendon Press, New York, 329 p.

Pistre, V., T. Kinoshita, T. Endo, K. Schilling, J. Pabon, B. Sinha, T. Plona, T. Ikegami, and D. Johnson, 2005, A modular wireline logging sonic tool for measurement of 3D (Azimuthal, radial and Axial) formation acoustic properties: SPWLA 46th annual logging symposium, New Orleans, 26-29 June 2005.

Pitmen, J., L. Price, and J. LeFever, 2001, Diagenesis and fracture development in Bakken Formation, Williston Basin: Implications for reservoir quality in the middle member: US Geological Survey Professional Paper 1653, 19 p.

Plona, T., M. Kane, B. Sinha, J. Walsh, and O. Viloria, 2000, Using acoustic anisotropy: SPWLA 41st annual logging symposium, June 4-7.

Plona, T., B. Sinha, M. Kane, R. Shenoy, S. Bose, J. Walsh, T. Endo, T. Ikegami, and O. Skelton, 2002, Mechanical damage detection and anisotropy evaluation using dipole sonic dispersion analysis: SPWLA 43rd annual logging symposium, 2-5 June 2002.

Price, L., and J. LeFever, 1994, Dysfunctionalism in Williston Basin: The Mid-Madison/Bakken petroleum system: Bulletin of Canadian Petroleum Geology, v. 42, p. 187-218.

Sayers, C.M., 2005, Seismic anisotropy of shales: Geophysics, v. 64, p. 93-98.

Sayers, C.M., 1994, The elastic anisotropy of shales: Journal of Geophysical Research-B, Solid Earth, v. 99, p. 767-774.

Shoenberg, M., Muir, F. and Sayers, C.M., 1996, Introducing ANNIE: a simple three parameters anisotropic velocity model for shales, Journal of Seismic Exploration, 5, 34-49.

Sinha, B., B. Vissapragada, L. Renlie, and S. Tysse, 2006, Radial profiling of the three formation shear moduli and its application to well completions: Geophysics, v. 71, p. E65-E77.

Sinha, B., B. Vissapragada, A. Wendt, M. Kongslien, H. Eser, E. Skomedal, L. Renile, and E. Pedersen, 2007, Estimation of formation stresses using radial variation of three shear moduli- a case study from a high-pressure, high-temperature reservoir in Norwegian continental shelf: SPE/ATCE, Convention, Anaheim, California, 11-14 November 2007.

Sinha, B., B. Vissapragada, L. Renlie, and S. Tysse, 2005, Radial profiling of three formation shear moduli: SEG, 75th annual meeting expanded abstracts, p. 364-368.

Tatham, R.H., M.D. McCormack, E.B. Neitzel, and D.F. Winterstein, 1991, Multicomponent seismology in petroleum exploration: Society of Exploration Geophysicists, Tulsa, Oklahoma, 248 p.

Thomsen, L., 1986, Weak elastic anisotropy: Geophysics, v. 51, p. 1954-1966.

Tsvankin, I., 2005, Seismic signatures and analysis of reflection data in anisotropic media: Elsevier science, second edition.

Tsvankin, I., 1997, Reflection move-out and parameter estimation for horizontal transverse isotropy: Geophysics, 62, 614-629.

Vernik, L., and X. Liu, 1997, Velocity anisotropy in shales - A petrophysical study: Geophysics, v. 62, p. 521-532.

Walsh, J., B. Sinha, and A. Donald, 2006, Formation anisotropy parameters using borehole sonic data: SPWLA 74th annual logging symposium, 4-7 June 2006.

Walsh, J., B. Sinha, T. Plona, D. Miller, and D. Bently, 2007, Derivation of anisotropy parameters in a shale using borehole sonic data: SEG 77th annual meeting, expanded abstract.

Ye, Fang, 2010, Sensitivity of seismic reflections to variations in anisotropy in the Bakken Formation, Williston Basin, North Dakota: Master's thesis, University of Texas at Austin, Austin, Texas, online resource, 109 p.

	Density(gr/cc)	C33-MPsi	C44-MPsi	C55-MPsi	C66-MPsi	C11(ANNIE_C55)-MPsi	C11(ANNIE_C44)-MPsi
UB	2.16	2.59	0.87	0.88	1.62	4.17	4.20
MB	2.61	8.58	2.90	2.96	2.97	8.61	8.72
LB	2.18	2.53	0.82	0.84	1.44	3.74	3.77

Table 1. Stiffness coefficients of Well A in three members of Bakken Formation.

	Epsilon(ANNIE_C44)	Epsilon(ANNIE_C55)	Gamma(C44)	Gamma(C55)
UB	0.23	0.22	0.29	0.25
MB	-0.01	-0.02	-0.01	-0.03
LB	0.14	0.12	0.21	0.17

Table 2. Thomsen anisotropy parameters of Well A in three members of Bakken Formation.

	C11(ANNIE_C44)-MPsi	C11(ANNIE_C55)-MPsi	C33-MPsi	C44-MPsi	C55-MPsi	C66-MPsi	Density(g/cc)
UB	4.69	4.57	3.19	1.08	1.14	1.70	2.31
MB	8.55	8.37	8.78	3.01	3.10	2.92	2.62
LB	4.34	4.21	3.37	1.16	1.23	1.65	2.28

Table 3. Stiffness coefficients of Well B in three members of Bakken Formation.

	Epsilon(ANNIE_C44)	Epsilon(ANNIE_C55)	Gamma(C44)	Gamma(C55)
UB	0.305	0.299	0.467	0.450
MB	0.009	0.003	0.014	0.004
LB	0.262	0.256	0.409	0.392

Table 4. Thomsen anisotropy parameters of Well B in three members of Bakken Formation
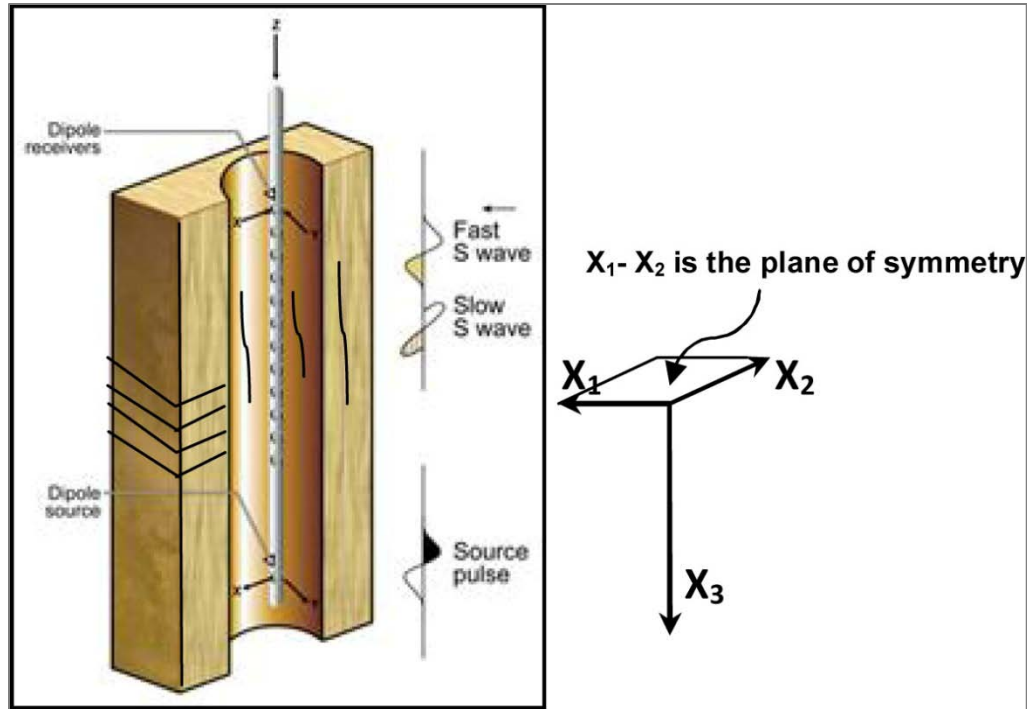
Figure 1. Well coordination in a VTI medium (Modified from Haldorsen et al., 2006).
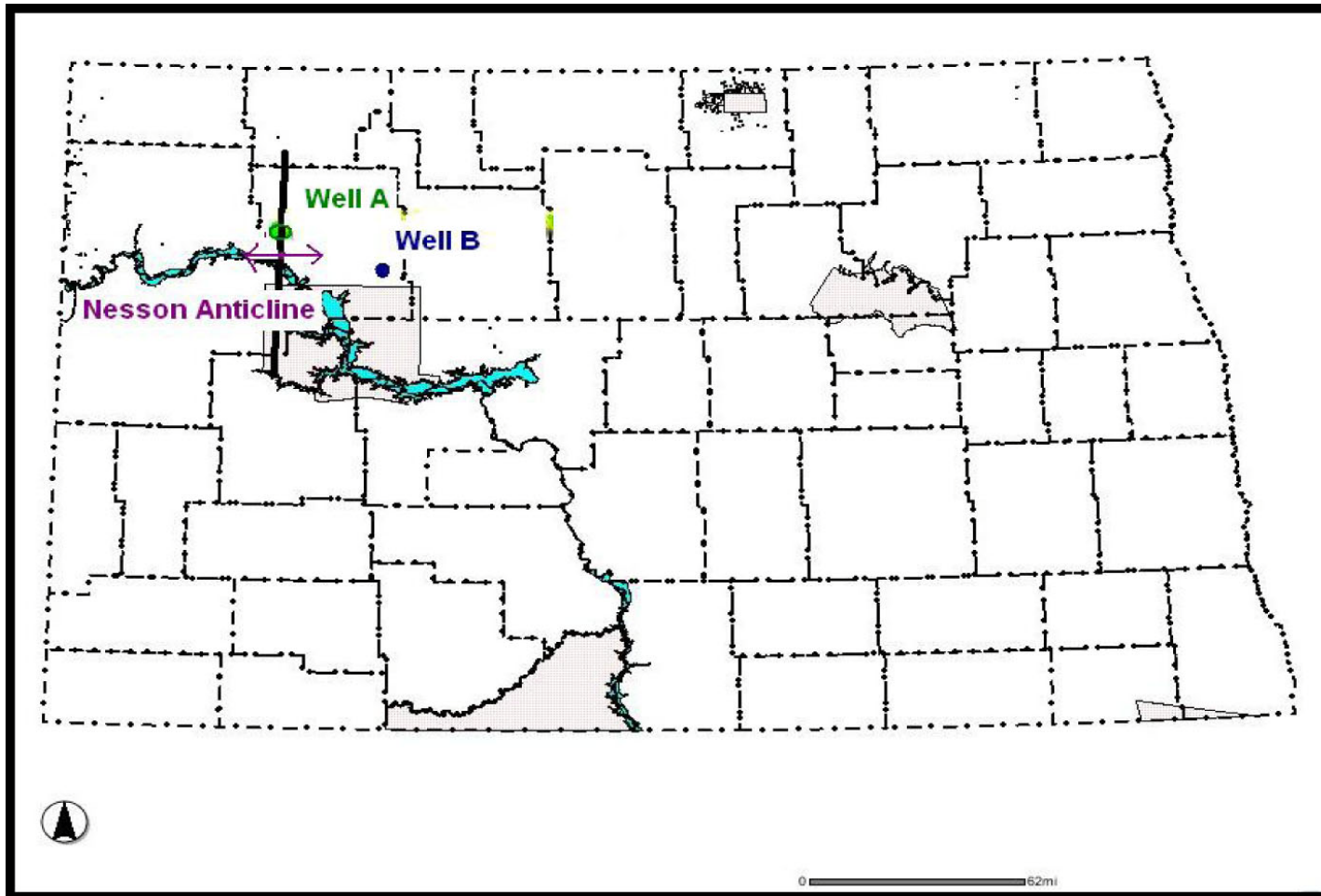
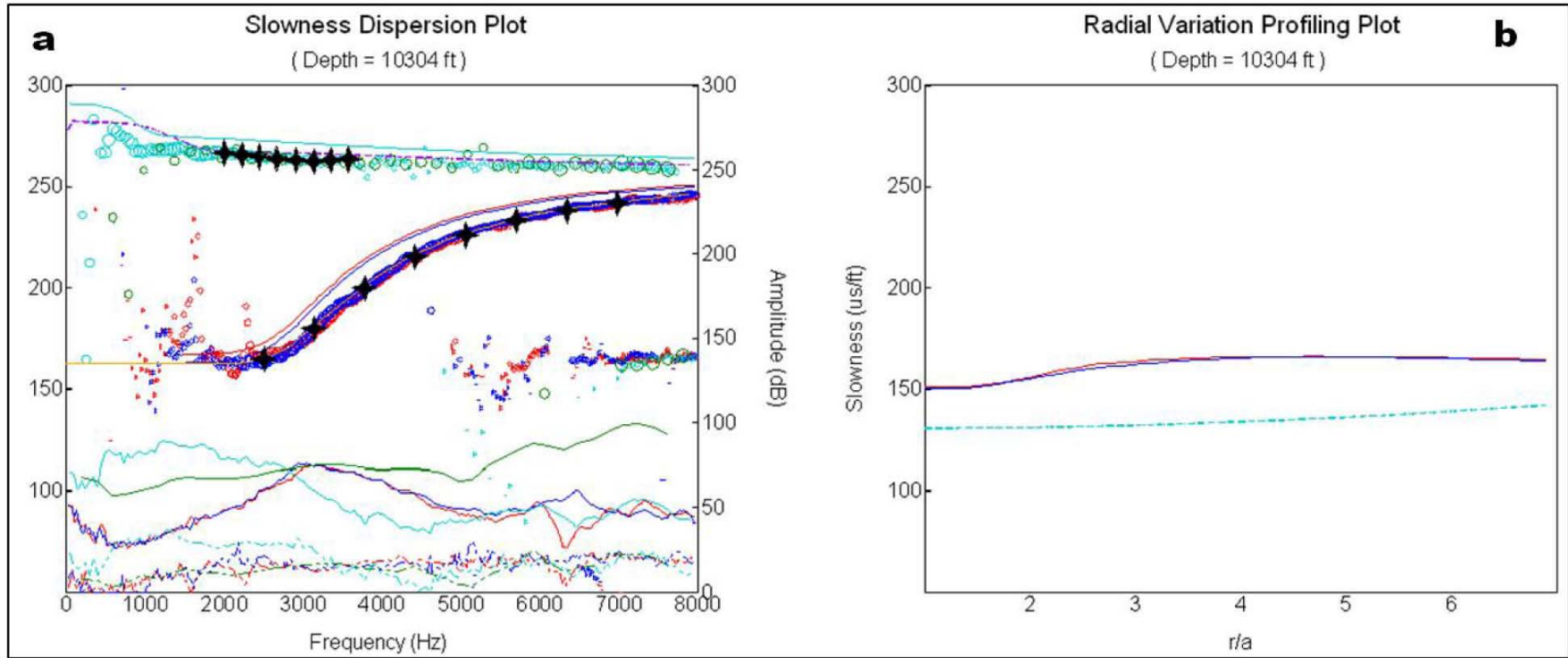Figure 2. Well locations (A and B) in North Dakota part of Williston Basin.

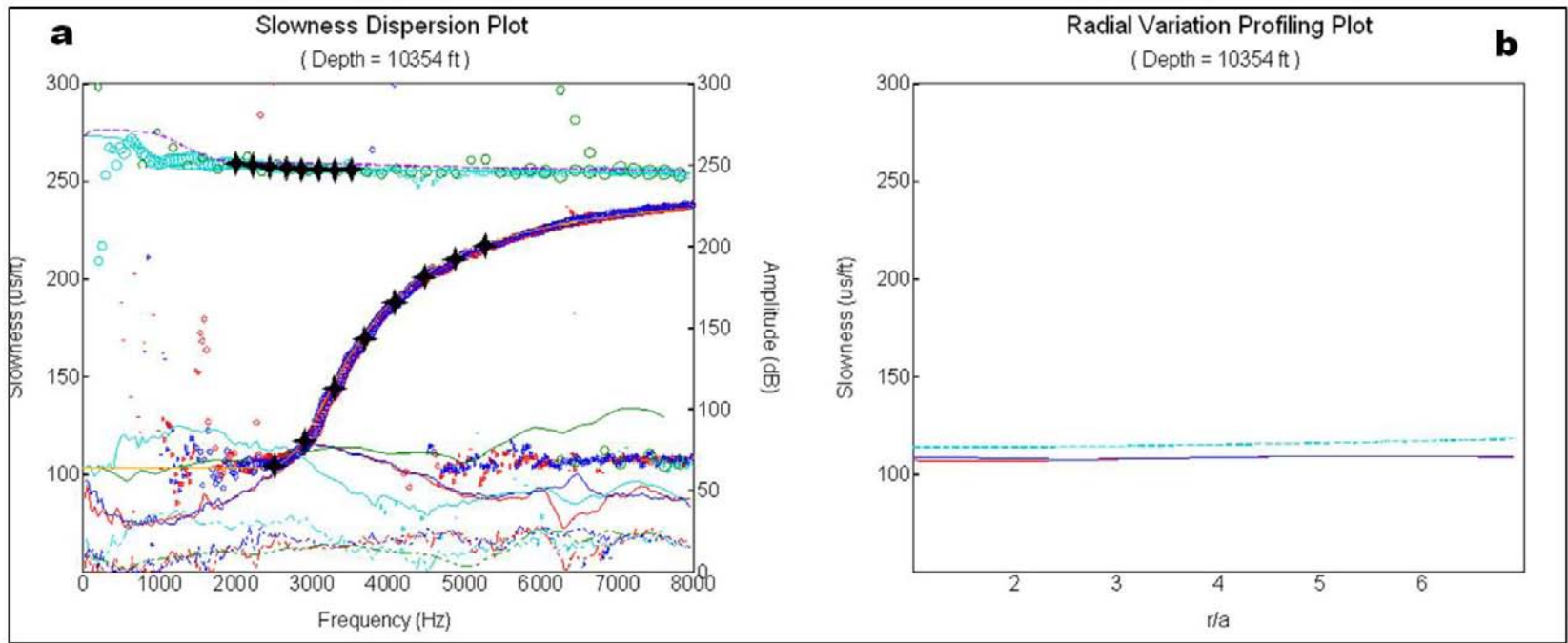Figure 3. Dispersion plot (a) and radial slowness variation profile (b) for Upper Bakken in Well A.

Figure 4. Dispersion plot (a) and radial slowness variation profile (b) for Middle Bakken in Well A.
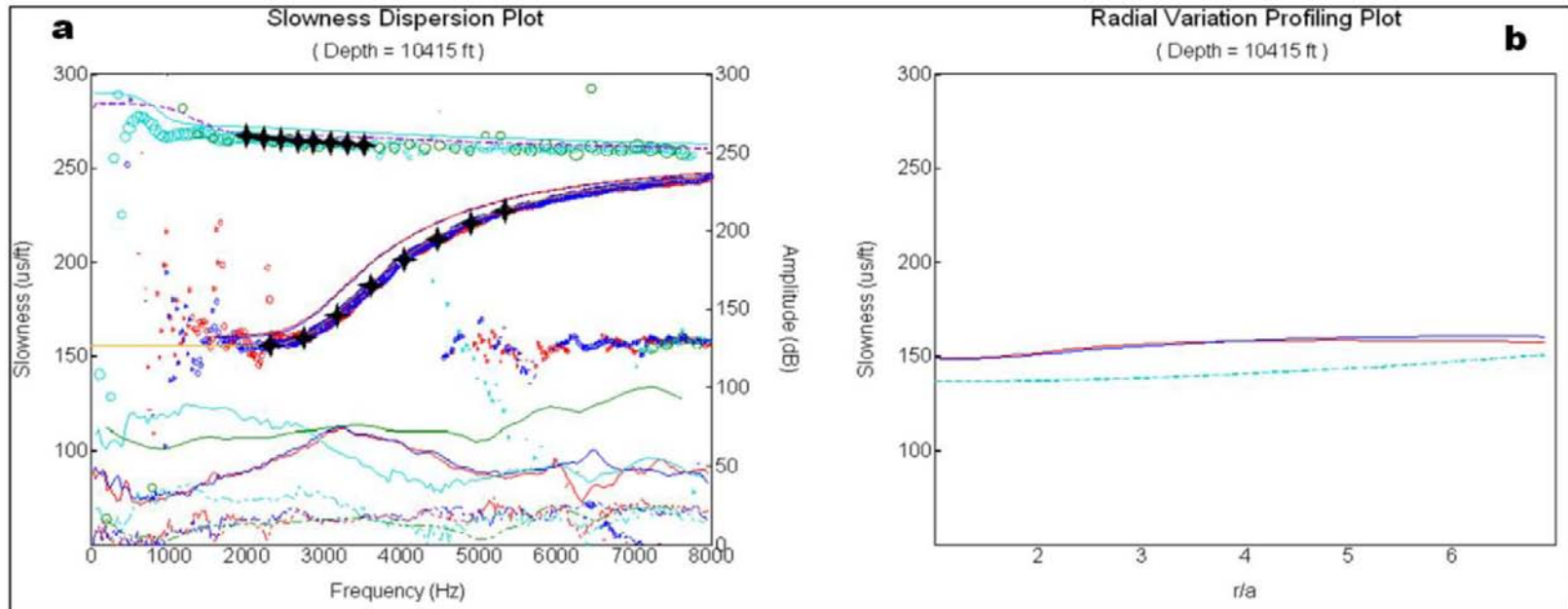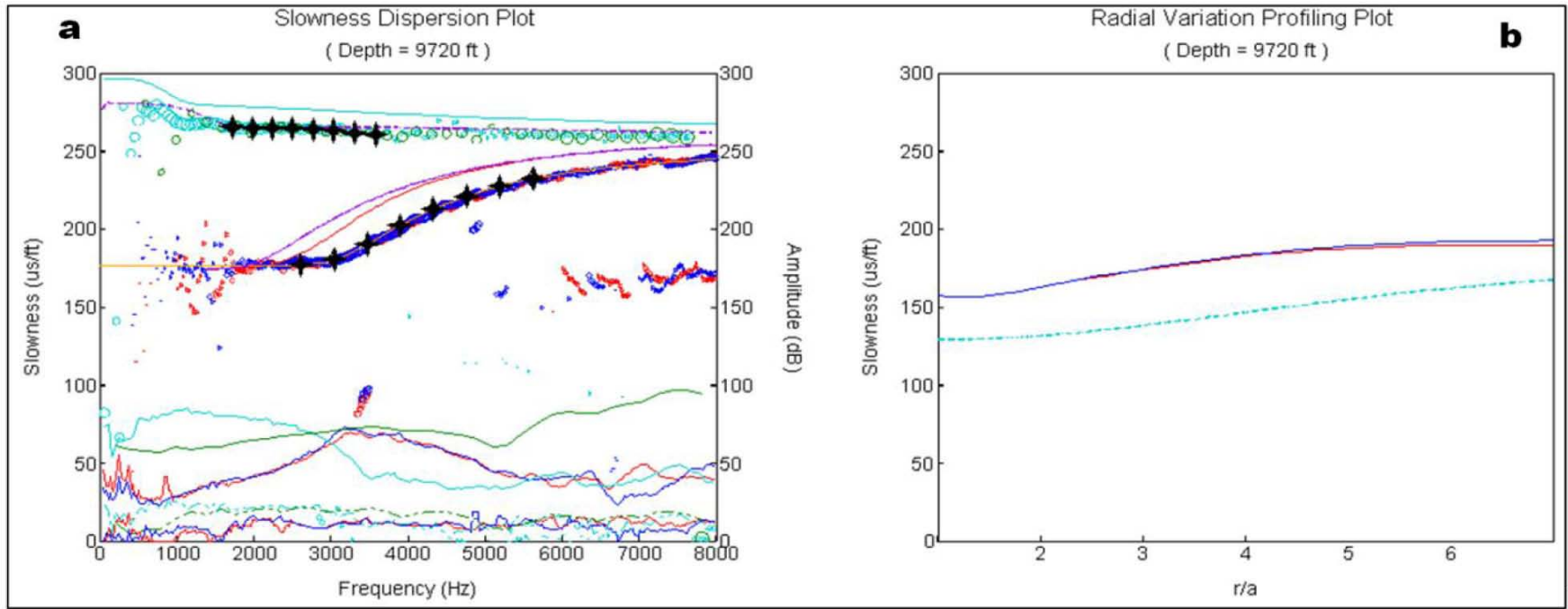
Figure 5. Dispersion plot (a) and radial slowness variation profile (b) for Lower Bakken in Well A.

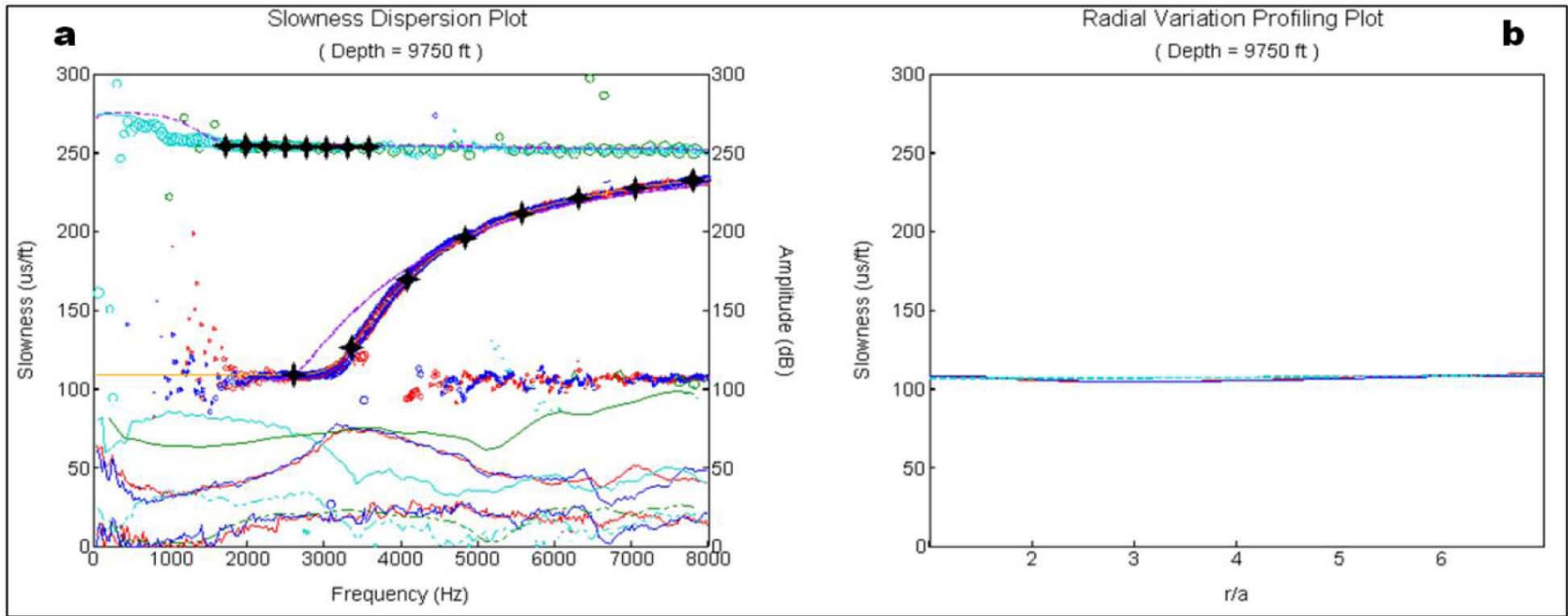Figure 6. Dispersion plot (a) and radial slowness variation profile (b) for Upper Bakken in Well B.

Figure 7. Dispersion plot (a) and radial slowness variation profile (b) for Middle Bakken in Well B.
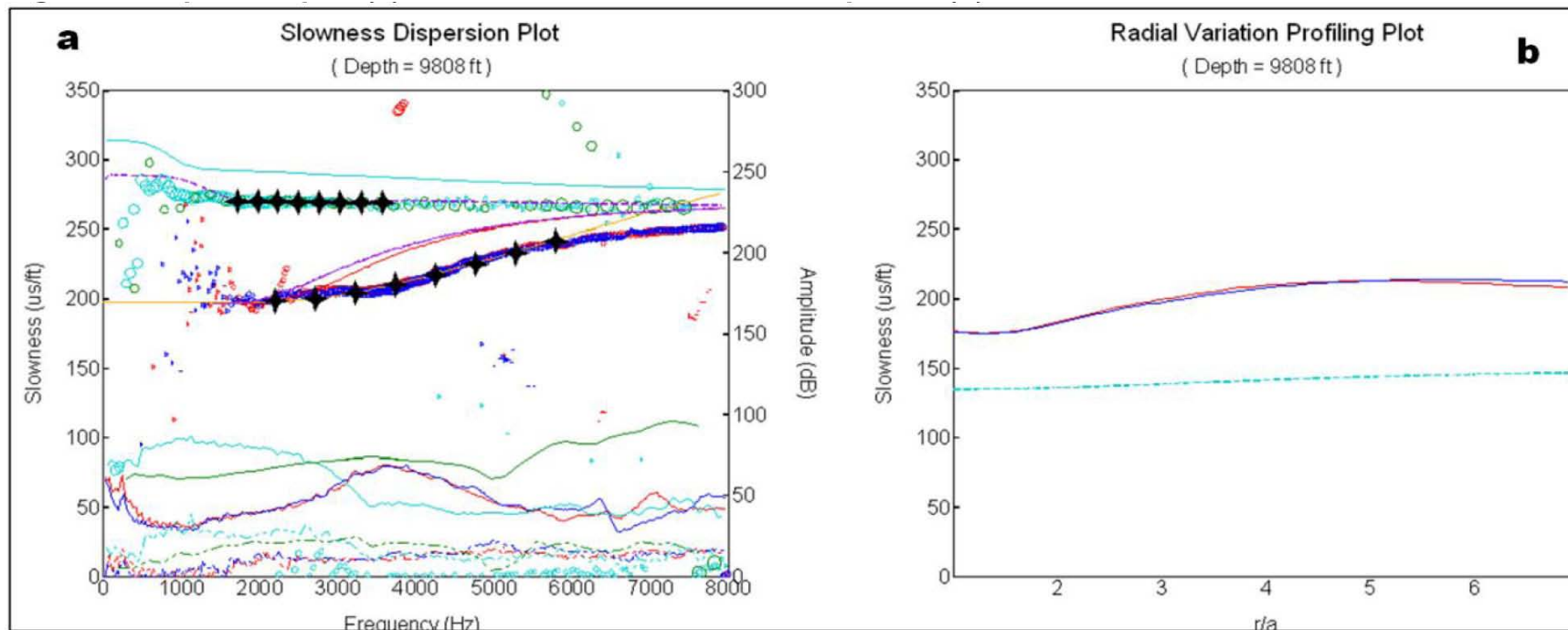
Figure 8. Dispersion plot (a) and radial slowness variation profile (b) for Lower Bakken in Well B.